

Density Fluctuations and Energy Spectra of 3D Bacterial Suspensions

Zhengyang Liu, Wei Zeng, Xiaolei Ma, and Xiang Cheng*

*Department of Chemical Engineering and Materials Science,
University of Minnesota, Minneapolis, MN 55455, USA*

(Dated: December 19, 2020)

We experimentally study density fluctuations and energy spectra of three-dimensional (3D) bacterial suspensions over a wide range of bacterial concentrations. Our results quantitatively verify the predicted scaling law of giant number fluctuations in 3D wet active fluids. Moreover, we show that such a scaling behavior persists at small scales even in low-concentration suspensions well before the transition to active turbulence. Our measurements on the energy spectra of bacterial suspensions support the theoretical prediction on the flow of dilute pusher swimmers and reveal the characteristic turbulent energy spectra of dense bacterial suspensions in the bulk limit. We also examine the density-flow coupling in both the steady and transient states of active turbulence. A universal density-independent and scale-invariant correlation between giant number fluctuations and energy spectra is found across multiple length scales. Our systematic experiments verify important theoretical predictions on density fluctuations and turbulent flow structures of 3D wet active fluids and provide new insights into the emergent dynamics of bulk bacterial suspensions.

I. INTRODUCTION

Active fluids exhibit many unusual behaviors beyond the expectation of equilibrium statistical mechanics [1–5]. In particular, an active fluid can exhibit anomalously large density variations, the so-called giant number fluctuations (GNF), where the standard deviation of the number of particles ΔN grows nonlinearly with the square root of the mean particle number \sqrt{N} , defying the central limit theorem of equilibrium systems [6]. Such unusual density fluctuations have been observed in a wide range of active fluids in both living and non-living systems including vibrated granular rods [7–10], swarming bacteria [11, 12] and mammalian cells [13], self-propelled cytoskeleton [14], and synthetic colloidal swimmers [15, 16]. Hence, GNF is generally viewed as a hallmark of the emergent behaviors of active fluids.

Although significant progress has been made in the theoretical understanding of GNF over the past two decades [17–29], systematic experiments that can quantitatively verify theoretical and numerical predictions are still few and far between. Particularly, the existing experiments on GNF all focused on dry two-dimensional (2D) or quasi-2D systems [7–15], where particle-boundary interactions play a significant role in affecting the density fluctuations of 2D active fluids [3]. Such system-specific interactions lead to a variety of scaling behaviors of GNF defined via $\Delta N/\sqrt{N} \sim N^\alpha$. A wide range of the scaling exponent α between 0.13 and 0.5 has been reported in different 2D experiments. In comparison, measurements of GNF in 3D wet active fluids, where hydrodynamics dominate the interparticle interactions and conserve the total momentum of systems, have not been achieved heretofore. As a result, experimental verification of the prediction of GNF in 3D wet active fluids without the influence of system boundaries is still out of reach. Important

questions such as how the long-ranged hydrodynamic interactions and the dimensionality of systems affect the density fluctuations of active fluids have not been properly addressed experimentally.

The rise of GNF in active fluids is usually accompanied by the transition to ordered phases with collective motion [1, 3]. For wet active fluids such as bacterial suspensions, the collective motion lead to large-scale coherent flows with intermittent vortices and jets, which are often referred to as active turbulence [30–39]. Similar to GNF that manifests density fluctuations across different scales, the flow of active turbulence also exhibits scale-dependent structures. Imported from the study of classical turbulence, energy spectra are frequently used to quantify such scale-dependent structures in active turbulence [31, 32, 37, 40–43]. Nevertheless, current experimental studies of energy spectra were limited to active turbulence at high particle concentrations. A systematic measurement of energy spectra over a broad range of particle concentrations is still lacking. More importantly, although both GNF and energy spectra quantify the scale-dependent dynamics of active fluids, the intrinsic connection between these two quantities across different scales has not been investigated.

Here, we present our systematic experimental study of GNF and energy spectra in bulk bacterial suspensions, a premier example of 3D wet active fluids [3]. Our experiments on GNF in high-concentration bacterial suspensions quantitatively verify the theoretical prediction on the scaling behavior of density fluctuations in 3D wet active fluids. More surprisingly, we find that such a scaling relation persists at small scales even in low-concentration suspensions well below the transition concentration of active turbulence. Such an unusual behavior arises due to the long-range nature of hydrodynamic interactions, lacking in 2D dry systems. Our systematic measurements on the energy spectra of bacterial suspensions of different concentrations further illustrate the emergence of the characteristic flow structure of active turbulence

* xcheng@umn.edu

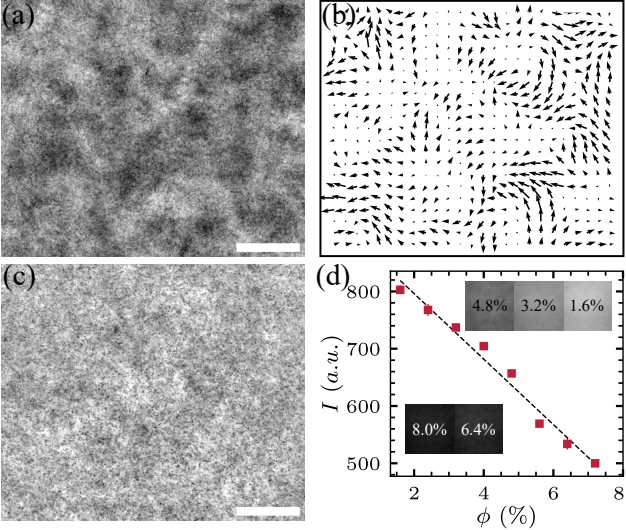


FIG. 1. Density fluctuations and active turbulence. (a) A snapshot of a dense suspension of *E. coli* with bacterial volume fraction $\phi = 6.4\%$. (b) 2D velocity field of the suspension shown in (a), which exhibits characteristic active turbulent flow patterns. (c) A snapshot of a dilute suspension of *E. coli* with $\phi = 1.6\%$, which shows no active turbulent flows. Scale bars are $85 \mu\text{m}$. (d) Average pixel intensities of images, I , as a function of ϕ . Inset shows the images of bacterial suspensions of different ϕ under the same light illumination.

and verify the prediction of the energy spectra of dilute pusher suspensions. Lastly, our experiments also reveal a density-independent and scale-invariant coupling between GNF and energy spectra. Quantitatively similar coupling has also been uncovered in the kinetic process during the transition towards active turbulence. Taken together, our study provides a solid experimental benchmark on density fluctuations and energy spectra of 3D bacterial suspensions and reveals an unexpected correlation between GNF and energy spectra across different length scales. Our experiments provide not only the first verification on several important theoretical predictions including the scaling law of GNF in 3D wet active fluids, the energy spectra of dilute pusher swimmers and the delayed onset of density fluctuations, but also new insights into the emergent dynamics of bulk bacterial suspensions such as local bacterial correlation in dilute suspensions and the universal coupling between density fluctuations and flow energies in the steady and transient states of active turbulence.

II. EXPERIMENT

We use genetically engineered light-powered *Escherichia coli* (*E. coli*) as our model bacteria (see Appendix A). For a typical experiment, a bacterial suspension of control volume fraction ϕ is injected into a sealed chamber of $20 \text{ mm} \times 3 \text{ mm} \times 140 \mu\text{m}$. We calculate

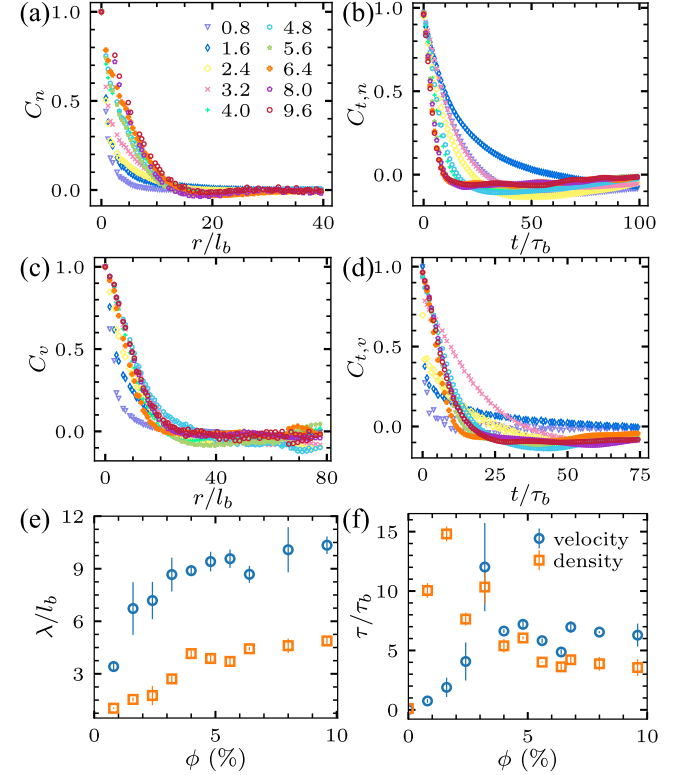


FIG. 2. Density and velocity spatiotemporal correlations. (a) Two-point density correlations at different bacterial volume fractions ϕ . Radial position r is normalized by the average length of bacteria $l_b = 3 \mu\text{m}$. (b) Density autocorrelations at different ϕ . Time t is normalized by the characteristic swimming time of bacteria $\tau_b = 0.2 \text{ s}$. (c) Two-point velocity correlations at different ϕ . (d) Velocity autocorrelations at different ϕ . ϕ (%) of different curves are indicated in (a). (e) Density and velocity correlation lengths, λ , versus ϕ . (f) Density and velocity correlation times, τ , versus ϕ .

$\phi = nV_b$, where n is the number density of bacteria and $V_b = \pi(w_b/2)^2 l_b = 1 \mu\text{m}^3$ is the average volume of a bacterium, where $l_b = 3 \mu\text{m}$ and $w_b = 0.65 \mu\text{m}$ are the average length and width of bacterial body. The volume of bacterial flagella is too small to affect the volume of bacteria. Without supply of oxygen, bacteria quickly consume all the oxygen in the chamber and stop moving after 5 minutes. We then illuminate the suspension with a high-intensity microscope light, which powers bacteria at their maximal swimming speed of $v_0 = 15 \pm 3 \mu\text{m/s}$ in the dilute limit. A video of the suspension is taken $50 \mu\text{m}$ above the bottom wall of the chamber by a bright-field inverted microscope at a frame rate of 30 fps with the field of view of $420 \times 360 \mu\text{m}^2$ (Fig. 1a). We use a standard Particle Image Velocimetry (PIV) algorithm to extract the 2D in-plane velocity field (v_x, v_y) in the 3D suspension [44]. The suspension exhibits the characteristic chaotic vortices and jets of active turbulence at high ϕ (Fig. 1b).

It is challenging to directly count the number of bacte-

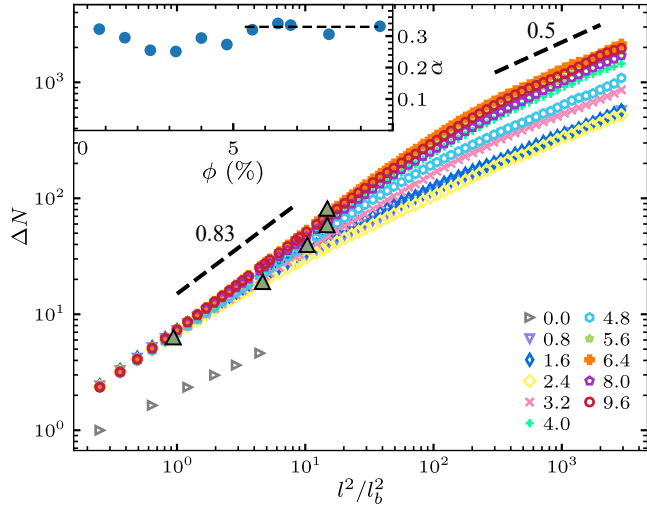


FIG. 3. Giant number fluctuations (GNF) for suspensions of different volume fractions ϕ . The standard deviation of particle number ΔN as a function of the scaled subsystem size l^2/l_b^2 . Dark green triangles indicate the density correlation lengths $\lambda(\phi)$ from Fig. 2e. Black dashed lines indicate a power-law scalings of 0.83 and 0.5 at small and large length scales, respectively. Inset: Scaling exponent α versus ϕ . α are extracted by fitting the experimental data from $0.3l_b$ to $\lambda(\phi)$. The dashed line in the inset indicates the theoretical prediction of $\alpha = 0.33$.

ria in a 3D dense suspension of fast moving bacteria. Luckily, by virtue of Beer-Lambert law, the local bacterial density is monotonically correlated with the local intensity of microscope images, where darker regions correspond to higher bacterial densities (Fig. 1a, c and Supplementary Video). Such a principle has been exploited in previous experiments in probing the dynamics of bacterial suspensions and actin filaments [14, 45, 46]. To calibrate the density-intensity correlation, we prepare bacterial suspensions of different ϕ and image the suspensions under the same illumination (Fig. 1d inset). The mean image intensity decreases with increasing ϕ following an approximately linear relation (Fig. 1d), agreeing with the the Beer-Lambert law for samples of small thickness and weak absorptivity appropriate for our experiments. The linear density-intensity relation has already been used in previous experiments on *E. coli* suspensions [46].

III. RESULTS

A. Density fluctuations

The simple linear relation allows us to measure the spatiotemporal evolution of local bacterial densities and investigate density fluctuations in 3D bacterial suspensions. We first calculate the two-point density spatial correlation, C_n , and the density auto-correlation, $C_{t,n}$, for suspensions of different ϕ (Fig. 2a, b) and compare

them with the well-studied velocity spatiotemporal correlations, C_v and $C_{t,v}$, extracted from PIV (Fig. 2c, d).

The correlation length λ and correlation time τ are determined when the corresponding normalized correlation functions decay to $1/e$ (Fig. 2e, f). Figure 2e shows the density correlation length λ at different ϕ , which quantifies the scale of density inhomogeneities in suspensions. λ is small at low ϕ , gradually increases with ϕ and reaches a plateau of $\sim 5l_b$ in high-concentration bacterial suspensions when $\phi > \phi_c$. Here, $\phi_c = 3.2\%$ is the transition concentration above which suspensions show active turbulence [39]. The velocity correlation length follows a qualitatively similar trend and also saturates above ϕ_c , consistent with previous finding [47]. The saturated velocity correlation length is about twice of the saturated density correlation length, which is determined by the size of system [34]. Figure 2f further compares the density and velocity correlation times, τ , at different ϕ . Although the density and velocity correlation times at low ϕ show a large discrepancy, they both plateau when $\phi > \phi_c$ at $\sim 5\tau_b$, where $\tau_b = l_b/v_0 = 0.2$ s is the characteristic swimming time scale of *E. coli*. The saturated velocity correlation time is slightly larger than the saturated density correlation time. The similarity between the density and the velocity correlation functions at high ϕ indicates a strong coupling between density fluctuations and active turbulent flows, a feature we shall examine in more details in Sec. III C across different length scales.

We further examine GNF by calculating the standard deviation of bacterial number ΔN and the mean bacterial number N in subsystems of increasing sizes [48]. $\Delta N/\sqrt{N}$ as a function of l^2/l_b^2 for bacterial suspensions of different ϕ is plotted in Fig. 3, where l is the side length of square subsystems. Note that since the depth of field of our images is fixed, the area of the subsystem l^2 is linearly proportional to the average number of particles N in the subsystem at a fixed ϕ . At a given ϕ , $\Delta N/\sqrt{N}$ plateaus when l is significantly larger than the density correlation length at the corresponding ϕ , $\lambda(\phi)$ (Fig. 2e). The central limit theorem applies at large length scales owing to the spatial average over multiple dense and dilute regions. Nevertheless, at small length scales when l is comparable or smaller than $\lambda(\phi)$, bacterial suspensions of all ϕ in our study exhibit obvious GNF, where $\Delta N/\sqrt{N}$ increases with increasing subsystem size. Remarkably, $\Delta N/\sqrt{N}$ versus l^2 approaches the same scaling in the small l limit even for low- ϕ suspensions without turbulent flows. Such a surprising finding is in contrast to GNF of 2D active systems, where GNF diminishes with decreasing particle concentrations [7–11, 14]. Kinetic theories have predicted that, due to the long-range hydrodynamic interactions, pusher-type microswimmers in 3D active suspensions show strong spatial and temporal correlations at low concentrations well below the transition concentration to active turbulence [49, 50]. Although the theories discussed the effect of the correlation on the enhanced diffusion of passive tracers and velocity fluctuations in dilute suspensions, our experiments show

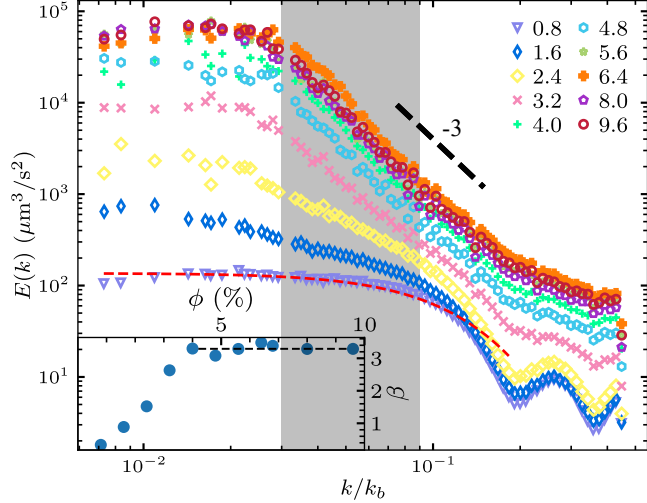


FIG. 4. Energy spectra $E(k)$ of bacterial suspensions of different volume fractions ϕ . Shaded region indicates the range over which the scaling exponent β is fitted. Black dashed line indicates a power-law scaling of -3 . Red dashed line is a fitting of $E(k)$ at $\phi = 0.8\%$ using Eq. 1. In the fitting, the bacterial number density $n = \phi V_b$ and the dipole length $l_d = 1.9 \mu\text{m}$ are from experiments, whereas the dipole strength $\kappa = 100 \mu\text{m}^3/\text{s}$ and the regularization length $\epsilon = 14 \mu\text{m}$ are taken as fitting parameters. In comparison, $\kappa = 300.8 \mu\text{m}^3/\text{s}$ from experiments (see text). Inset: Scaling exponent of $E(k)$, β , as a function of ϕ . Dashed line indicates $\beta = 3.3$.

that such a correlation also manifests as GNF at small length scales in low concentration bacterial suspensions.

Quantitatively, the strength of GNF can be measured by the scaling exponent α following $\Delta N/\sqrt{N} \sim N^\alpha$. $\alpha = 0$ for equilibrium systems obeying the central limit theorem, whereas the upper bound $\alpha = 0.5$ corresponds to a system with maximal density fluctuations. We extract α by fitting the experimental curves with the power-law relation for $k < \lambda(\phi)$. The inset of Fig. 3 shows α as a function of ϕ , where α remains approximately constant at 0.30 ± 0.03 for all ϕ . In contrast, α decreases with decreasing ϕ for 2D GNF. Notably, for high $\phi \geq 5.6\%$, α stabilizes to 0.33 ± 0.01 , quantitatively agreeing with the theoretical prediction of $\alpha = 1/3$ for 3D suspensions of polar-ordered self-propelled particles with hydrodynamic interactions [20]. Hence, our experiments quantitatively verify the theory of the GNF of 3D wet active fluids. More interestingly, our study shows that the same GNF scaling persists in low concentration suspensions at small scales even before the emergence of large scale active turbulence.

B. Energy spectra

Similar to GNF, the velocity field of active turbulence also shows scale-dependent structures, which are often characterized by the energy spectrum of turbu-

lent flows, $E(k)$ [48]. $E(k)$ measures the kinetic energy density at different scales in terms of wavenumber $k = 2\pi/l$. It is related to the mean kinetic energy density $\langle v_x^2 + v_y^2 \rangle / 2 = \int_0^\infty E(k) dk$. Figure 4 shows $E(k)$ of bacterial suspensions at different ϕ . $E(k)$ of low- ϕ suspensions with uncorrelated pusher swimmers has been predicted [36]

$$E(k) = 4\pi n \kappa^2 \left[\frac{1}{3} + \frac{\cos(kl_d)}{(kl_d)^2} - \frac{\sin(kl_d)}{(kl_d)^3} \right] \frac{\epsilon^4 k^2}{l_d^2} K_2^2(k\epsilon), \quad (1)$$

where n is the number density of bacteria, κ is the dipole strength and l_d is the dipolar length of *E. coli*. ϵ is the distance for the regularization of the dipolar flow field. K_2 is the modified Bessel function of the second kind. The fitting of Eq. 1 agrees well with our experimental $E(k)$ at low ϕ in the small k limit (Fig. 4). Particularly, Eq. 1 dictates that $E(k)$ is flat as $k \rightarrow 0$, a key feature confirmed by our experiments. A simple dimensional analysis can show that the plateau $E(k)$ at the small k follows $\lim_{k \rightarrow 0} E(k) \sim nk^2$ for uncorrelated swimmers of density n . The dipole strength can be estimated as $\kappa = Fl_d/\eta = \xi v_0 l_d/\eta = 300.8 \mu\text{m}^3/\text{s}$, where η is the viscosity of the buffer. ξ is the drag coefficient of a bacterial body orientated along its major axis, which can be calculated based on the body geometry $\xi = 3\pi\eta w_b [1 - (1 - l_b/w_b)/5]$ [51]. $l_d = 1.9 \mu\text{m}$ is from direct measurements [52]. Thus, $\lim_{k \rightarrow 0} E(k) = 7 \times 10^2 \mu\text{m}^3/\text{s}$, within the same order as our experiments. The discrepancy between Eq. 1 and experiments at large k may arise from the strong bacterial correlation at small length scales as shown by density fluctuations, as well as potential PIV errors due to the small number of bacteria in each PIV box of low- ϕ suspensions.

With increasing ϕ , $E(k)$ at small k increases sharply. In the turbulent regime at high ϕ , the kinetic energy is concentrated at scales much larger than the size of single bacteria, even though the turbulent flow is entirely driven by the swimming of single bacteria. The overall trend of $E(k)$ with increasing ϕ qualitatively agrees with the results from large-scale particle simulations [26, 36].

We also extract the scaling exponent β of $E(k) \sim k^{-\beta}$ by fitting the energy spectra at intermediate k , where a significant change of $E(k)$ with ϕ occurs and $E(k)$ exhibits good power-law relations. β increases with ϕ and saturates at 3.3 ± 0.1 at high $\phi > \phi_c$. The saturated scaling exponent is quantitatively similar to that obtained from the active turbulence of high-concentration sperm suspensions at large k [42]. The exponent is also consistent with experiments on confined dense suspensions of *B. subtilis*, where the scaling of $E(k) \sim k^{-8/3}$ has been reported at large k [31]. Since the characteristic size of turbulent vortices as quantified by the velocity correlation length is linearly proportional to the system size L [34], when k is significantly smaller than $2\pi/L$, $E(k)$ would decrease, exhibiting the non-monotonic trend shown in [31]. The large system size of $L = 140 \mu\text{m}$ of our experiments allows us to probe the small k limit

predicted by theories and simulations without the influence of system boundaries.

Although the scaling in the small k limit is strongly affected by the system size, the scaling in the large k limit seems to be universal with $\beta \approx 3$ from different experiments. To the best of our knowledge, no theoretical prediction has been made on this universal scaling behavior for 3D active turbulence. Giomi investigated the energy spectra of 2D active nematics by combining numerical simulations with mean-field theories and showed $E(k) \sim k^{-4}$ in the large k limit [41]. The result has also been confirmed recently by a hydrodynamic theory [37]. For isotropic turbulence in d dimension, the energy spectra can be written as $E(k) = C_d k^{d-1} \langle \mathbf{v}(\mathbf{k}) \cdot \mathbf{v}(-\mathbf{k}) \rangle_{k=|\mathbf{k}|}$ [31, 36], where $C_d k^{d-1}$ is the surface area of $(d-1)$ -sphere and $\langle \mathbf{v}(\mathbf{k}) \cdot \mathbf{v}(-\mathbf{k}) \rangle_{k=|\mathbf{k}|}$ is the Fourier transform of the velocity-velocity spatial correlation function. If the velocity correlation function for 2D active nematics is qualitatively similar to that of 3D bacterial suspensions independent of the dimensionality of systems, the mean-field theory would then predict a scaling of $E(k) \sim k^{-3}$, consistent with experimental observations. Such a hypothesis, although intriguing, is certainly non-trivial and needs further theoretical investigation. Note that although we measure the energy spectra of 2D in-plane flows of 3D suspensions, the scaling of the spectra is determined by the spectra of 3D turbulent flows [53]. Taken together, our study provides systematic experiments on the evolution of $E(k)$ over a large range of ϕ in bulk bacterial suspensions. The results verify the existing theory on low-concentration active pusher suspensions and serve as a benchmark for future theoretical development on the spectral properties of 3D active turbulence.

C. Density-flow coupling

Both GNF and energy spectra probe the scale dependence of active bacterial suspensions. The former measures density fluctuations at different scales, whereas the latter considers the transfer of flow energies across scales. Although both properties have been extensively studied, a direct correlation between the two has not been explicitly examined heretofore. Indeed, the quantitative similarity between the density spatiotemporal correlations and the velocity spatiotemporal correlations shown in Fig. 2 has already indicated a strong density-flow coupling in the turbulent regime. Moreover, the trends of GNF and energy spectra also show similar characteristics, both exhibiting a rapid increase at small length scales and plateaus at large length scales (Figs. 3 and 4). Such a similarity suggests that a density-independent correlation between density fluctuations and kinetic energies may exist across different length scales. To verify the hypothesis, we plot density fluctuations $\Delta N/\sqrt{N}$ against the corresponding kinetic energy densities $E(k)$ at the same scale in Fig. 5a. We find that all the $\Delta N/\sqrt{N}$ - E pairs in the turbulent regime fall onto a master curve

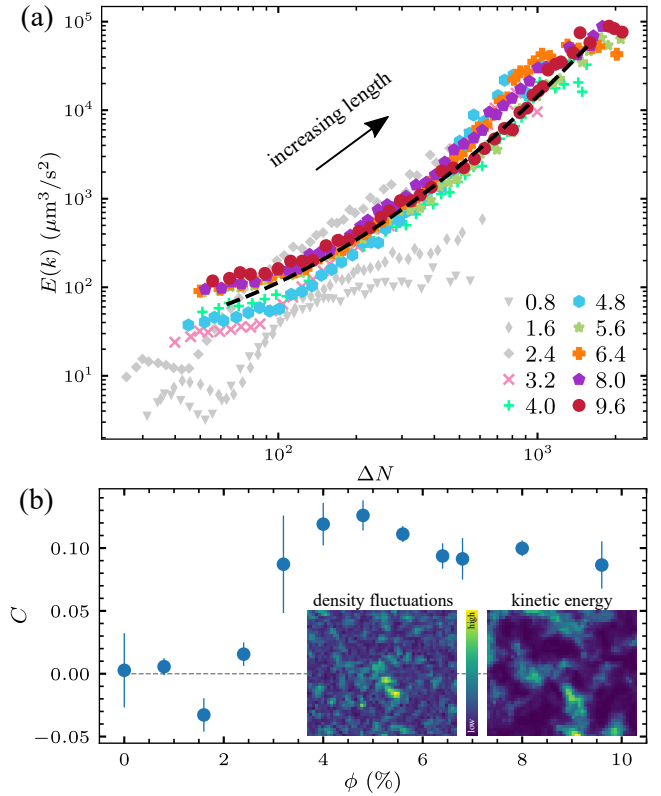


FIG. 5. Coupling between density fluctuations and kinetic energies. (a) Energy spectra $E(k)$ plotted against number density fluctuations ΔN at each corresponding length scale for bacterial suspensions of different volume fractions ϕ . Gray symbols are used for low- ϕ suspensions without active turbulence. Black dashed line is a polynomial fitting of the master curve, serving as guide for the eye. Black arrow indicates the direction of increasing lengths. (b) Correlation of local density fluctuations and kinetic energies C as a function of ϕ . Inset: snapshots of a density fluctuation field and a kinetic energy field for a bacterial suspension of $\phi = 4.8\%$.

over multiple length scales extending from the size of PIV boxes up to a macroscopic length a few times larger than the density correlation length, regardless of the volume fractions of the samples. In comparison, $\Delta N/\sqrt{N}$ - E shows much larger scattering for low ϕ suspensions without active turbulence. Although it is not surprising that density fluctuations should correlate with kinetic energies in general as both measure different aspects of the same active turbulence, the collapse of data from samples of different volume fractions is quite unexpected. The results show that the coupling between density fluctuations and turbulent flows occur at every scale of active turbulence in a quantitative same fashion. Such a scale-invariant coupling is independent of the volume fraction of bacterial suspensions.

To illustrate such an unusual coupling in real space, we calculate the *local* correlation of density fluctuations and kinetic energies at a randomly selected length scale

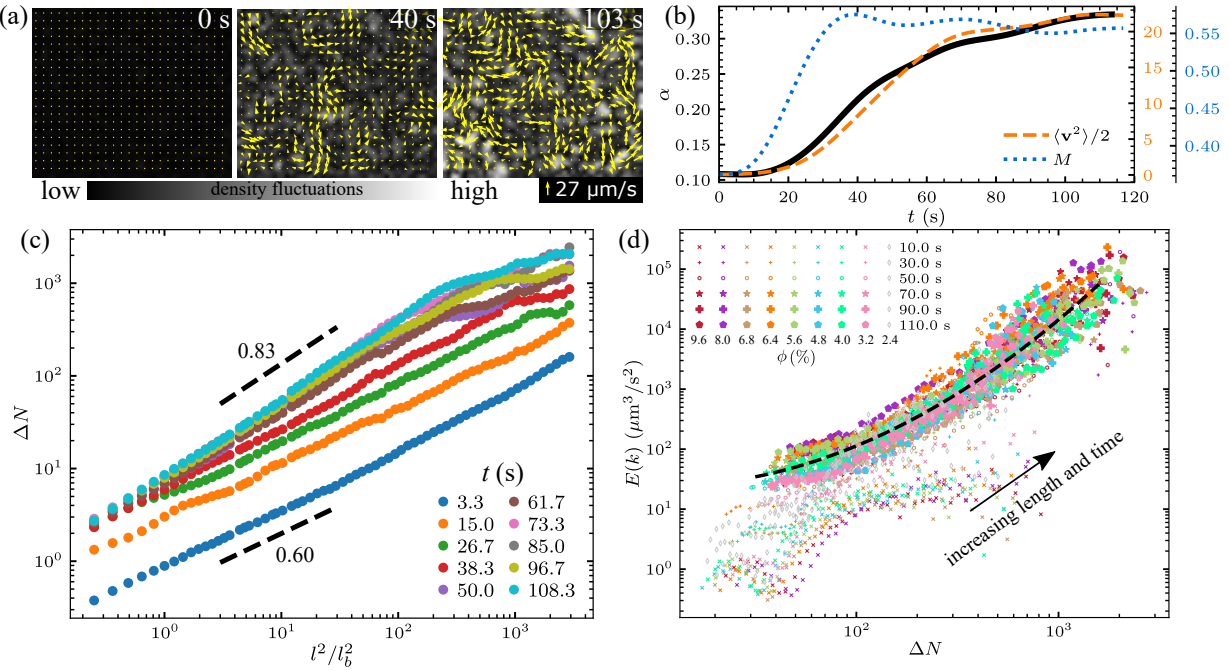


FIG. 6. Transient density-flow coupling during the transition towards active turbulence. (a) Snapshots of a bacterial suspension of volume fraction $\phi = 6.4\%$ during the transition towards active turbulence. Background gray scale indicates the magnitude of local density fluctuations. Yellow arrows show the velocity fields obtained from PIV analysis. The light is turned on at time $t = 0$. (b) Temporal evolution of the GNF scaling exponent α , the total kinetic energy $\langle v^2 \rangle / 2$ and the area fraction of regions with collective flow M from the same transition process shown in (a). (c) Growth of ΔN in the bacterial suspension. t are indicated in the legend in unit of seconds. (d) Energy spectra $E(k)$ versus GNF ΔN during the active turbulent transition. t and ϕ are encoded in the marker shapes and color, respectively. The black dashed line is the fitting of the master curve shown in Fig. 5a.

of $l = 2.5l_b$. The local density fluctuation $\delta N(\mathbf{r}, t)$ and local kinetic energy $E(\mathbf{r}, t)$ at position $\mathbf{r} = (x, y)$ and time t are extracted from the image intensity field and the PIV velocity field, respectively (Fig. 5b inset) [48]. The normalized correlation between $\delta N(\mathbf{r}, t)$ and $E(\mathbf{r}, t)$ averaged over all \mathbf{r} and t is then computed at different ϕ (Fig. 5b). At low ϕ without active turbulence, the correlation is weak and fluctuates around zero, which then increases sharply with ϕ as bacterial suspensions transition to active turbulence. A constant positive correlation is found in the turbulent regime when $\phi > \phi_c$. This real-space measurement provides a concrete example of the coupling between density fluctuations and turbulent kinetic energy at small scales.

More surprisingly, we find that the same density-flow coupling also exists in the kinetic process during the transition towards bacterial turbulence. Taking the advantage of the light-powered bacteria, we trigger the onset of bacterial turbulence by suddenly turning on the light illumination on high- ϕ bacterial suspensions at $t = 0$ [39]. The snapshots of a bacterial suspension of $\phi = 6.4\%$ through the transition are shown in Fig. 6a, which are overlaid with the flow fields obtained from PIV. At $t = 0$, local flow velocities are random close to 0. At $t = 40$ s, although the kinetic energy of the flow is still low, the

direction of velocities align locally, exhibiting the characteristic collectively moving vortices and jets of active turbulence. At $t = 103$ s, kinetic energy grows significantly and saturates. The suspension reaches the steady state of active turbulence.

We monitor the temporal evolution of density fluctuations and energy spectra of the suspension in the transient state before the suspension reaches the steady turbulence. Figure 6c shows the growth of GNF during the turbulent transition. Different from the steady-state GNF at different ϕ , where strong GNF persists at small length scales even for low- ϕ suspensions, the high- ϕ bacterial suspension shows no or very weak GNF at the onset of active turbulence at small t , with the scaling exponent $\alpha \approx 0.11$ at early times. The strength of GNF gradually increases over time, as indicated by the smooth increase of $\alpha(t)$ (the black line in Fig. 6b). α saturates to the steady state value of 0.33 above $t \approx 90$ s. Interestingly, the growth of GNF is significantly delayed compared with the formation of collective turbulent flows, which is measured by the area fraction of the regions with strong local velocity alignment, M [39, 48, 54]. M reaches a plateau at a much earlier time around 30 s (the blue dotted line in Fig. 6b). The finding provides strong experimental evidence to an important prediction of the kinetic theory

of active fluids [55, 56], where density fluctuations are shown to be the consequence of the nonlinear development of the hydrodynamic instability of pusher swimmers and appear only at long times. In the linear regime, at the onset of the hydrodynamic instability with the initial rise of the collective turbulent flow, density fluctuations should remain weak. In contrast to the separation of the time scales of M and α , we find that the growth of α and the kinetic energy E are strongly coupled and show quantitatively similar trends (the black and the orange lines in Fig. 6b), clearly demonstrating the density-energy coupling in the kinetic process.

Lastly, we analyze the correlation between GNF $\Delta N/\sqrt{N}$ and energy spectra $E(k)$ during the turbulent transition for bacterial suspensions of different ϕ (Fig. 6d). When $\phi > \phi_c$, all the data at different t , ϕ and l collapse into the same master curve obtained from the steady-state measurements [48]. The result suggests that kinetic energies control not only the steady-state GNF but also the rise of GNF at different length scales.

IV. CONCLUSIONS

We have conducted systematic experiments measuring density fluctuations and energy spectra of 3D bacterial suspensions over a wide range of concentrations in both the steady and transient states. The scaling behavior of the number density fluctuation $\Delta N/\sqrt{N} \sim N^\alpha$ observed in our experiments was in quantitative agreement with the theoretical prediction on the giant number fluctuations of suspensions of polar-ordered self-propelled particles. More importantly, we showed that such a scaling behavior persisted at small lengths in low-concentration suspensions well below the transition concentration to active turbulence. The finding provided new experimental evidence on the existence of strong local bacterial correlation in dilute suspensions due to

the long-range hydrodynamic interactions of 3D wet active fluids. In addition to density fluctuations, we also examined the energy spectra of bacterial suspensions of different concentrations. Our results quantitatively verified the prediction of the energy spectra of dilute pusher-type active fluids and illustrated the emergence of the characteristic energy spectra of active turbulence in dense bacterial suspensions in the bulk limit without the confinement effect. Lastly, our detailed analysis of the density and velocity fields at different scales revealed a profound coupling between density fluctuations and kinetic energies across different scales ranging from the size of single bacteria to the correlation length of large-scale collective flows. Such a density-independent and scale-invariant coupling was also uncovered in the kinetic process during the transition towards bacterial active turbulence. This density-flow coupling resulted in the delay of the onset of giant number fluctuations with respect to the rise of the collective turbulent flows, supporting a key prediction of the kinetic theory. As such, our study provided a comprehensive experimental benchmark on the density fluctuations and energy spectra of 3D bacterial suspensions and shed new light onto the emergent dynamics of wet active fluids.

ACKNOWLEDGMENTS

We thank D. Ghosh, Y. Peng, Y. Qiao and K. Zhang for the help with experiments and fruitful discussions. The research is supported by NSF CBET 1702352, NSF CBET 2028652 and the Packard foundation.

Appendix A: Materials and methods

-
- [1] S. Ramaswamy, *Annu. Rev. Condens. Matter Phys.* **1**, 323 (2010).
 - [2] M. E. Cates, *Reports Prog. Phys.* **75**, 42601 (2012).
 - [3] M. C. Marchetti, J. F. Joanny, S. Ramaswamy, T. B. Liverpool, J. Prost, M. Rao, and R. A. Simha, *Rev. Mod. Phys.* **85**, 1143 (2013).
 - [4] W. C. K. Poon, in *Proceedings of the International School of Physics "Enrico Fermi", Course CLXXXIV "Physics of Complex Colloid"*, edited by F. S. C. Bechinger and P. Zicherl (ISO Press, 2013).
 - [5] J. Elgeti, R. G. Winkler, and G. Gompper, *Reports Prog. Phys.* **78**, 056601 (2015).
 - [6] Y. Mishin, *Ann. Phys. (N. Y.)* **363**, 48 (2015).
 - [7] V. Narayan, S. Ramaswamy, and N. Menon, *Science* **317**, 105 (2007).
 - [8] I. Aranson, A. Snezhko, J. S. Olafsen, and J. S. Urbach, *Science* **320**, 612 (2008).
 - [9] A. Kudrolli, G. Lumay, D. Volfson, and L. S. Tsimring, *Phys. Rev. Lett.* **100**, 2 (2008).
 - [10] J. Deseigne, O. Dauchot, and H. Chaté, *Phys. Rev. Lett.* **105**, 1 (2010).
 - [11] H. P. Zhang, A. Be'er, E. L. Florin, and H. L. Swinney, *Proc. Natl. Acad. Sci. U. S. A.* **107**, 13626 (2010).
 - [12] D. Nishiguchi, K. H. Nagai, H. Chaté, and M. Sano, *Phys. Rev. E* **95**, 1 (2017).
 - [13] K. Kawaguchi, R. Kageyama, and M. Sano, *Nature* **545**, 327 (2017).
 - [14] V. Schaller and A. R. Bausch, *Proc. Natl. Acad. Sci. U. S. A.* **110**, 4488 (2013).
 - [15] J. Palacci, S. Sacanna, A. P. Steinberg, D. J. Pine, and P. M. Chaikin, *Science* **339**, 936 (2013).
 - [16] H. Karani, G. E. Pradillo, and P. M. Vlahovska, *Phys. Rev. Lett.* **123**, 208002 (2019).
 - [17] J. Toner and Y. Tu, *Phys. Rev. Lett.* **75**, 4326 (1995).

- [18] Y. Tu, J. Toner, and M. Ulm, *Phys. Rev. Lett.* **80**, 4819 (1998).
- [19] J. Toner and Y. Tu, *Phys. Rev. E* **58**, 4828 (1998).
- [20] R. Aditi Simha and S. Ramaswamy, *Phys. Rev. Lett.* **89**, 58101 (2002).
- [21] S. Ramaswamy, R. A. Simha, and J. Toner, *Europhys. Lett.* **62**, 196 (2003).
- [22] J. Toner, Y. Tu, and S. Ramaswamy, *Ann. Phys. (N. Y.)* **318**, 170 (2005).
- [23] H. Chaté, F. Ginelli, G. Grégoire, and F. Raynaud, *Phys. Rev. E* **77**, 046113 (2008).
- [24] S. Mishra, A. Baskaran, and M. C. Marchetti, *Phys. Rev. E* **81**, 061916 (2010).
- [25] S. Dey, D. Das, and R. Rajesh, *Phys. Rev. Lett.* **108**, 1 (2012).
- [26] D. Saintillan and M. J. Shelley, *J. R. Soc. Interface* **9**, 571 (2012).
- [27] D. Saintillan and M. J. Shelley, *Comptes Rendus Phys.* **14**, 497 (2013).
- [28] S. Ngo, A. Peshkov, I. S. Aranson, E. Bertin, F. Ginelli, and H. Chaté, *Phys. Rev. Lett.* **113**, 1 (2014).
- [29] B. Mahault, F. Ginelli, and H. Chaté, *Phys. Rev. Lett.* **123**, 1 (2019).
- [30] C. W. Wolgemuth, *Biophys. J.* **95**, 1564 (2008).
- [31] H. H. Wensink, J. Dunkel, S. Heidenreich, K. Drescher, R. E. Goldstein, H. Löwen, and J. M. Yeomans, *Proc. Natl. Acad. Sci. U. S. A.* **109**, 14308 (2012).
- [32] J. Dunkel, S. Heidenreich, K. Drescher, H. H. Wensink, M. Bär, and R. E. Goldstein, *Phys. Rev. Lett.* **110**, 1 (2013).
- [33] V. Bratanov, F. Jenko, and E. Frey, *Proc. Natl. Acad. Sci. U. S. A.* **112**, 15048 (2015).
- [34] S. Guo, D. Samanta, Y. Peng, X. Xu, and X. Cheng, *Proc. Natl. Acad. Sci. U. S. A.* **115**, 7212 (2018).
- [35] M. Linkmann, G. Boffetta, M. C. Marchetti, and B. Eckhardt, *Phys. Rev. Lett.* **122**, 214503 (2019).
- [36] D. Bardfalvy, H. Nordanger, C. Nardini, A. Morozov, and J. Stenhammar, *Soft Matter* **15**, 7747 (2019).
- [37] R. Alert, J. F. Joanny, and J. Casademunt, *Nat. Phys.* **16**, 682 (2020).
- [38] V. Škultéty, C. Nardini, J. Stenhammar, D. Marenduzzo, and A. Morozov, *Phys. Rev. X* **10**, 1 (2020).
- [39] Y. Peng, Z. Liu, and X. Cheng, Imaging the emergence of bacterial turbulence using light-powered escherichia coli (2020), arXiv:2003.12399 [cond-mat.soft].
- [40] T. Ishikawa, N. Yoshida, H. Ueno, M. Wiedeman, Y. Imai, and T. Yamaguchi, *Phys. Rev. Lett.* **107**, 1 (2011).
- [41] L. Giomi, *Phys. Rev. X* **5**, 031003 (2015).
- [42] A. Creppy, O. Praud, X. Druart, P. L. Kohnke, and F. Plouraboué, *Phys. Rev. E* **92**, 032722 (2015).
- [43] A. E. Patteson, A. Gopinath, and P. E. Arratia, *Nat. Commun.* **9**, 5373 (2018).
- [44] A. Liberzon, D. Lasagna, M. Aubert, P. Bachant, T. Käufer, jakirkham, A. Bauer, B. Vodenicharski, C. Dallas, J. Borg, tomerast, and ranleu, *OpenPIV* (2020).
- [45] A. Sokolov, R. E. Goldstein, F. I. Feldchtein, and I. S. Aranson, *Phys. Rev. E* **80**, 1 (2009).
- [46] L. G. Wilson, V. A. Martinez, J. Schwarz-Linek, J. Tailleur, G. Bryant, P. N. Pusey, and W. C. K. Poon, *Phys. Rev. Lett.* **106**, 7 (2011).
- [47] A. Sokolov, I. S. Aranson, J. O. Kessler, and R. E. Goldstein, *Phys. Rev. Lett.* **98**, 158102 (2007).
- [48] See Supplemental Material.
- [49] J. Stenhammar, C. Nardini, R. W. Nash, D. Marenduzzo, and A. Morozov, *Phys. Rev. Lett.* **119**, 1 (2017).
- [50] S. Nambiar, P. Garg, and G. Subramanian, *Journal of Fluid Mechanics* **907**, A26 (2021).
- [51] Y. Magariyama and S. Kudo, *Biophysical Journal* **83**, 733 (2002).
- [52] K. Drescher, J. Dunkel, L. H. Cisneros, S. Ganguly, and R. E. Goldstein, *Proceedings of the National Academy of Sciences* **108**, 10940 (2011), <https://www.pnas.org/content/108/27/10940.full.pdf>.
- [53] S. B. Pope, *Turbulent Flows* (Cambridge Univ. Press, 2020).
- [54] L. H. Cisneros, J. O. Kessler, S. Ganguly, and R. E. Goldstein, *Phys. Rev. E* **83**, 061907 (2011).
- [55] D. Saintillan and M. J. Shelley, *Phys. Rev. Lett.* **100**, 1 (2008).
- [56] D. Saintillan and M. J. Shelley, *Phys. Fluids* **20**, 123304 (2008).